Geomechanics and Engineering, *Vol. 30, No. 2 (2022) 123-138*
https://doi.org/10.12989/gae.2022.30.2.123

Seismic bearing capacity of shallow embedded strip footing on rock slopes

Shuvankar Das[a], Koushik Halder[b] and Debarghya Chakraborty*

Department of Civil Engineering, Indian Institute of Technology Kharagpur, Kharagpur-721302, India

(Received August 10, 2021, Revised May 30, 2022, Accepted June 7, 2022)

Abstract. Present study computes the ultimate bearing capacity of an embedded strip footing situated on the rock slope subjected to seismic loading. Influences of embedment depth of strip footing, horizontal seismic acceleration coefficient, rock slope angle, Geological Strength Index, normalized uniaxial compressive strength of rock mass, disturbance factor, and Hoek-Brown material constant are studied in detail. To perform the analysis, the lower bound finite element limit analysis method in combination with the semidefinite programming is utilized. From the results of the present study, it can be found that the magnitude of the bearing capacity factor reduces quite substantially with an increment in the seismic loading. In addition, with the increment in slope angle, further reduction in the value of the bearing capacity factor is observed. On the other hand, with an increment in the embedment depth, an increment in the value of the bearing capacity factor is found. Stress contours are presented to describe the combined failure mechanism of the footing-rock slope system in the presence of static as well as seismic loadings for the different embedment depths.

Keywords: embedded footing; lower bound limit analysis; rock slope; seismic bearing capacity; semidefinite programming

1. Introduction

Several engineering structures like bridge abutments, transmission towers and roads are generally constructed near the sloping ground in hilly areas. In such areas, the material below the foundation is mostly rock. It is also known from the past that hilly areas are prone to earthquake events, which triggers instability in rock slope. Further, due to the construction of structural foundation on its crest, there is a high chance that rock slope may become unstable. Therefore, it becomes essential to determine the bearing capacity of the foundation on rock slope in the presence of seismic loading. In the past, the bearing capacity of strip footing near soil slope was determined by many researchers (Azzouz and Baligh 1983, Shields *et al.* 1990, Georgiadis 2010, Castelli and Lentini 2012, Keskin and Laman 2014, Shukla and Jakka 2018, Halder and Chakraborty 2020, Yang *et al*. 2021, Casablanca *et al.* 2021) in the presence of static as well as seismic forces. Meyerhof (1963) was the pioneer to consider the effect of embedment depth in a strip footing located on horizontal soil surface subjected to static loading. Later, a few researchers (Kumar and Ghosh 2006, Chakraborty and Kumar 2015, Wu *et al*. 2021) determined the bearing capacity factors of the embedded strip footing situated on soil slope under seismic loading condition. By incorporating an additional shear resistance between soil and the vertical sides of the footing, only few studies (Kumar and Ghosh 2006, Chakraborty and Kumar 2015) measured the seismic bearing capacity factors. However, to the best knowledge of the authors, there is no study available for the embedded strip footing situated on rock slope. Therefore, the bearing capacity of the embedded strip footing on rock slope is determined in the present study by considering the effects of static as well as seismic loadings. In the past, several researchers (Lyamin 1998, Yang *et al*. 2003, Merifield *et al*. 2006, Kumar and Mohapatra 2018, Alencar *et al*. 2019, Alencar *et al.* 2020) determined the bearing capacity factors of the strip footing placed on horizontal rock surface in the presence of static loading. Recently, Keshavarz *et al*. (2016) have presented the seismic bearing capacity of a strip footing on horizontal rock surface by implementing the slip line method. Moreover, from the past literature, it is found that limited studies (Yang 2009, Saada 2011, Ausilio and Zimmaro 2015, Maghous *et al*. 2020) are carried out to assess the seismic bearing capacity of the strip footing situated on rock slope only by considering the upper bound limit analysis with the help of the predefined failure surfaces. In the present study, by utilizing the lower bound finite element limit analysis (LB-FELA) in combination with the semidefinite programming (SDP), the bearing capacity of the embedded strip footing is determined in the presence of seismic loading. Unlike the past studies, no predefined failure surface is presumed, as the present study is carried out by utilizing the LB-FELA. The effect of seismic loading is applied into the analysis by following the pseudo-static approach (Sarma and Iossifelis 1990, Budhu and Al-Karni 1993, Kumar and Rao 2003, Baker *et al*. 2006, Karray *et al*. 2018). As the present study deals with the seismic event in

*Corresponding author, Ph.D.
E-mail: debarghya@civil.iitkgp.ac.in
[a]Ph.D. Student
E-mail: shuvankar.das@iitkgp.ac.in
[b]Ph.D.
E-mail: koushikhalder1410@gmail.com

ISSN: 2005-307X (Print), 2092-6219 (Online)

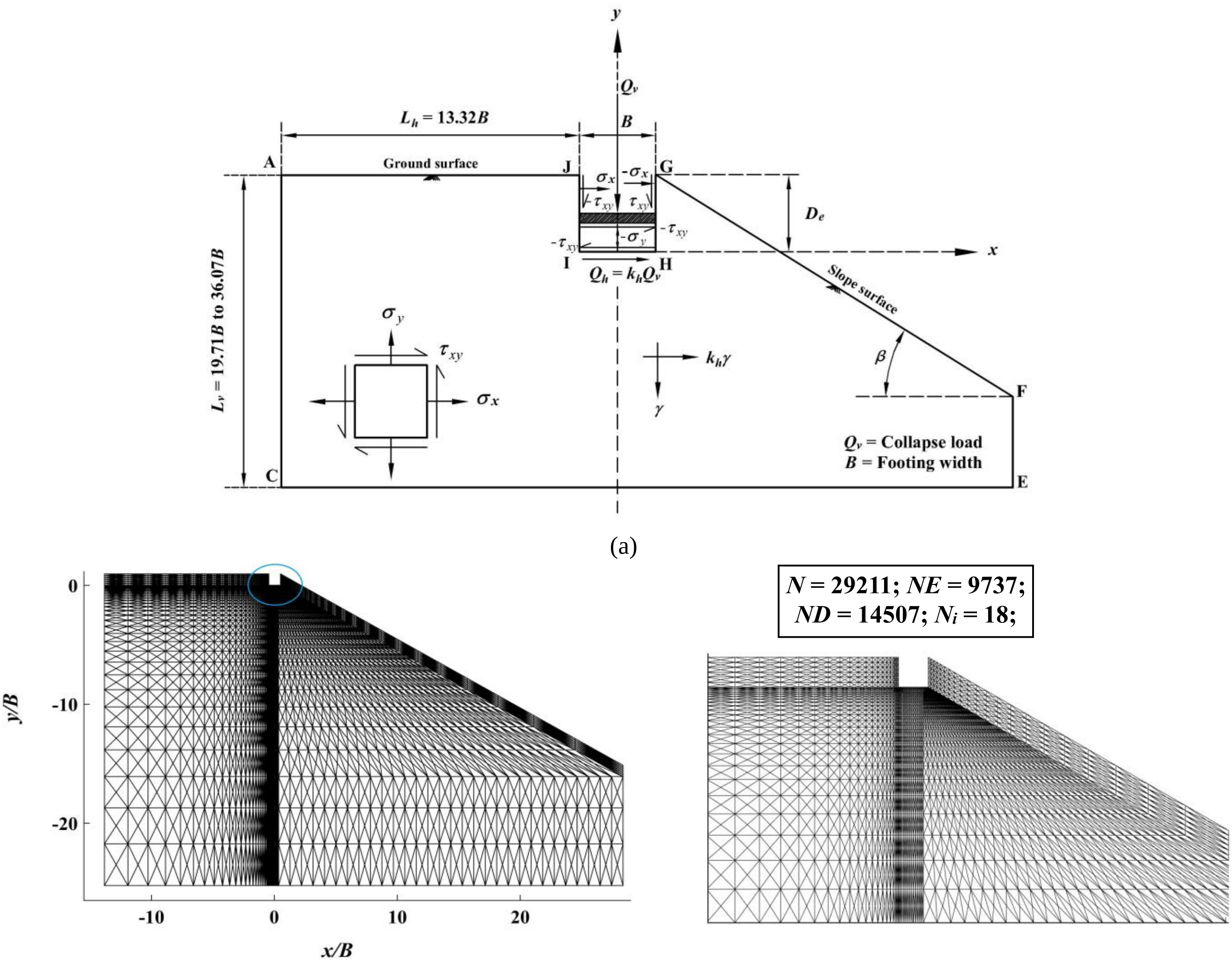

(b) (c)

Fig. 1 (a) Problem domain and stress boundary conditions; (b) finite element mesh used in the present study for GSI = 70, m_i = 25, D = 0, $\sigma_{ci}/\gamma B$ = 1000, and β = 30° and (c) zoomed view of mesh near footing

embedded strip footing, the shear resistance of rock mass, which is present above the footing level, is explicitly taken into the analysis. The effects of embedment depth (D_e), slope angle (β), horizontal seismic acceleration coefficient (k_h), and rock mass parameters (GSI, m_i, D, $\sigma_{ci}/\gamma B$) are inspected and presented in a series of design charts. Using these design charts, engineers can quickly estimate the bearing capacity of the foundation placed on the rock slope. The extent of the failure zone during collapse is also studied for different cases to examine the combined failure mechanism of the footing-rock slope system.

2. Problem definition

In the present study, by utilizing LB-FELA, the ultimate bearing capacity factor (N_σ) is evaluated for an embedded rigid strip footing of width B, situated on a rock slope edge in the presence of horizontal seismic acceleration $k_h g$, where g is the acceleration due to gravity. The rock slope makes an angle β with the horizontal axis. The schematic diagram is presented in Fig. 1(a). The rock mass is assumed to follow the Modified Hoek-Brown yield criterion. In the present study, the bearing capacity factor (N_σ) is expressed as

$$N_\sigma = \frac{(Q_v / B)}{\sigma_{ci}} \tag{1}$$

where Q_v = magnitude of the maximum vertical collapse load subjected to horizontal seismic acceleration; σ_{ci} = uniaxial compressive stress of intact rock.

3. Mesh details and stress boundary conditions

By considering the present study as a plane strain problem, the two-dimensional stress domain is selected in the x-y plane and illustrated in Fig. 1(a). The footing base-rock interface (IH) and footing wall-rock interfaces (JI and GH) are modeled as perfectly rough. The normal and shear stresses are assumed to be zero along the slope surface (GF) and top ground surface (AJ). No boundary conditions are implemented along the vertical boundaries (AC and EF) and the bottom horizontal boundary (CE). The domain in the vertical and horizontal directions is extended in such a way that the rock mass around the edges (AC, EF, and CE) do not yield, and the magnitude of collapse load does not change even if a larger size of the domain is selected. The extent of the domain varies from 19.71B to 36.07B in the vertical direction, and the width of the domain varies from 12.5B to 37.5B in the horizontal direction. The triangular elements having three nodes are applied to discretize the stress field. To find the stress distribution more accurately, denser mesh is created near the footing, and coarser mesh is generated near the boundary where the effect of the developed stresses due to the footing load is minimal. A typical finite-element mesh with GSI = 70, m_i = 25, D = 0, $\sigma_{ci}/\gamma B$ = 1000, D_e/B = 1, and β = 30° is shown in Fig. 1(b).

In Fig. 1(b), the notations NE, N, ND, and N_i indicate the total number of (1) elements, (2) nodes, (3) discontinuities, and (4) nodes along the interface of footing base-rock, respectively.

4. Methodology

As the present study is performed by utilizing the LB-FELA with the SDP, the basic formulation is derived from the studies of Lysmer (1970) and Sloan (1988). Thus, each node of the triangular element is assigned with three unknown nodal stresses (σ_x, σ_y, and τ_{xy}). In addition, the following four conditions also require to be fulfilled: (1) the element equilibrium equations, (2) the stress boundary conditions, (3) continuity of the shear and normal stresses across the common edges of two adjacent rock elements, and (4) the yield criterion. The steps for developing the constraint equations for element equilibrium, stress boundary, and stress discontinuity can be found in Sloan (1988). For rock mass, the well-accepted Generalized Hoek-Brown (GHB) yield criterion (Hoek *et al.* 2002) can be utilized to predict the failure. Recently, several studies (Xiao *et al.* 2019, Zhang *et al.* 2019, Rahaman and Kumar 2020) have been performed by embedding the GHB yield criterion into the finite element limit analysis. The application of this criterion is mostly suitable for the foundation on intact rock or heavily jointed rock masses (Merifield *et al.* 2006). The GHB yield criterion can be expressed as

$$\sigma_1-\sigma_3-\left(-(\sigma_{ci})^{\left(\frac{1}{\alpha}-1\right)}m_b\sigma_1+s(\sigma_{ci})^{\frac{1}{\alpha}}\right)^{\alpha}\le 0 \tag{2}$$

where σ_1 and σ_3 are the effective major and minor principal stresses. Here, m_b, α and s are the functions of (1) Geological Strength Index (GSI), (2) material constant (m_i), and (3) disturbance factor (D). In the present study, the normal tensile stress is considered as positive.

The above parameters are computed by utilizing the following relationships.

$$m_b=m_i\left(\frac{GSI-100}{28-14D}\right) \tag{3a}$$

$$s=\exp\left(\frac{GSI-100}{9-3D}\right) \tag{3b}$$

$$\alpha=\frac{1}{2}+\frac{1}{6}\left(e^{-\frac{GSI}{15}}-e^{-\frac{20}{3}}\right) \tag{3c}$$

where GSI varies between 10 (poor rock mass) and 100 (intact rock mass); m_i ranges from 1 to 35; to indicate the degree of disturbance in rock mass, the magnitudes of D ranges from 0 (undisturbed) to 1(highly disturbed). The value of the exponent α ranges from 0.59 to 0.50 for the magnitude of GSI from 10 to 100, respectively. By following the similar approach of Kumar and Mohapatra (2017), the present study is carried out by considering the value of the α as 0.5 to incorporate the semidefinite optimization and named as the Modified Hoek-Brown (MHB) yield criterion. Some recent studies (Kumar and Mohapatra 2017, Ukritchon and Keawsawasvong 2019a, Ukritchon and Keawsawasvong 2019b) have shown that the adopted approximation gives a consistent result for the GSI values between 30 and 100. A comparison of strength envelopes between the MHB and GHB yield criteria shows a good agreement, as illustrated in Fig. 2(a). Thus, by considering α = 0.5 in Eq. (2), the MHB yield criterion can be expressed as

$$\sigma_1-\sigma_3-\left(-\sigma_{ci}m_b\sigma_1+s\sigma_{ci}{}^2\right)^{0.5}\le 0 \tag{4}$$

As per the SDP framework, the maximum and minimum principal stresses, which are also the maximum and minimum eigenvalues of stress tensor (σ), can be expressed by following two semidefinite expressions

$$t_{\max}I-\sigma\succeq 0;\quad \sigma-t_{\min}I\succeq 0 \tag{5a}$$

$$\sigma=\begin{bmatrix}\sigma_x & \tau_{xy}\\ \tau_{xy} & \sigma_y\end{bmatrix} \tag{5b}$$

where I = Identity matrix of dimension 2 x 2; t_{max} and t_{min} are auxiliary variables; $t_{\max}\ge\sigma_1$ and $t_{\min}\le\sigma_3$. The operator '$\succeq$' indicates the semidefinite matrix condition. By using Eq. (5(a)), Eq. (4) can be rewritten as

$$t_{\max}-t_{\min}\le\left(-\sigma_{ci}m_b\sigma_1+s\sigma_{ci}{}^2\right)^{0.5} \tag{6}$$

By squaring both the left and right-hand sides, the terms in Eq. (6) are converted into a rotated quadratic conic constraint as expressed below

$$\xi_3^2\le 2\xi_1\xi_2 \tag{7a}$$

$$\text{Where }\ \xi_1=0.5;\ \xi_2=(-\sigma_{ci}m_b\sigma_1+s\sigma_{ci}^2);\quad \xi_3=t_{\max}-t_{\min};\ \xi_1\ge 0;\ \xi_2\ge 0 \tag{7b}$$

In the above expressions, ξ_1, ξ_2, and ξ_3 are auxiliary scalar variables. It is not allowed to input the Linear Matrix Inequality (LMI) equation directly into most of the SDP solvers. For that reason, two LMI equations are converted into linear equations by incorporating two slack variables, X and Y.

$$t_{\max} I - \sigma = X \; ; \;\; \sigma - t_{\min} I = Y \tag{7c}$$

By using Eqs. (7(a))-(7(c)), the MHB yield criterion can be expressed as

$$\begin{gathered}[A_1^{\mathrm{HB}}]\{\sigma\} + [A_2^{\mathrm{HB}}]\{t\} + [A_3^{\mathrm{HB}}]\{\xi\} + [A_4^{\mathrm{HB}}]\{X\} \\ + [A_5^{\mathrm{HB}}]\{Y\} = \{b^{\mathrm{HB}}\}\end{gathered} \tag{8a}$$

$$X \succeq 0 \; ; \qquad Y \succeq 0 \tag{8b}$$

Ultimately, Eqs. (8(a)) and (8(b)) can also be expressed as

$$\begin{gathered}[A_i^{\mathrm{HB}}]\{z\} = \{b^{\mathrm{HB}}\} \\ X \succeq 0 \; ; \quad Y \succeq 0 \\ \text{for } i = 1, 2, ..., 5\end{gathered} \tag{8c}$$

where $[A_1^{\mathrm{HB}}]$, $[A_2^{\mathrm{HB}}]$, $[A_3^{\mathrm{HB}}]$, $[A_4^{\mathrm{HB}}]$, $[A_5^{\mathrm{HB}}]$, and $\{b^{\mathrm{HB}}\}$ are the matrices and vector introduced for the implementation of the MHB yield criterion at each node of the element as a rotated quadratic conic constraint. Here, $\{t\}$ contains the vector of t_{max} and t_{min}; $\{X\}$ and $\{Y\}$ are the reshaped vectors from two-dimensional positive semidefinite matrixes X and Y, respectively; $\{\xi\}$ contains the vector of ξ_1, ξ_2, and ξ_3; $\{z\}$ is the global stress vector including auxiliary variables.

To incorporate the seismic force into the formulation, an equality constraint, $Q_h = k_h Q_v$ is applied, where Q_h is the integrated shear stresses along the nodes of the footing base-rock interface (IH) and normal stresses along the nodes of the footing wall-rock interfaces (JI and GH), as shown in Fig. 1(a). The reason behind the above equality equation is that, in the occurrence of horizontal seismic acceleration, an additional inertial force of magnitude $k_h Q_u$ occurs in the superstructure, where Q_u specifies the vertical ultimate collapse load acting at the footing base. It needs to be stated here that although, the present study is carried out only by considering the horizontal seismic force, the result of the present study is still applicable for the determination of the bearing capacity in the occurrence of both the vertical and horizontal seismic loadings. It can be done by following the modifications in the magnitude of the horizontal seismic acceleration coefficient and unit weight; a detailed description is presented in Appendix A.

4.1 Final form of the optimization problem

Finally, the expression for collapse load (i.e., the objective function) is formulated by integrating (1) the normal stresses acting in the nodes along the footing base-rock interface (IH), and (2) the shear stresses acting in the nodes along the footing wall-rock interfaces (JI and GH). After enforcing all the constraints (equilibrium, boundary, discontinuity, and yield), the collapse load is maximized by applying the SDP. After performing the required assembly of the constraints, the final form is expressed as an optimization problem.

$$\text{Maximize} \qquad \{p^T\}\{z\} \tag{9a}$$

$$\text{Subjected to} \qquad [A_g]\{z\} = \{b_g\} \; ; \;\; X \succeq 0 \; ; \;\; Y \succeq 0 \tag{9b}$$

where $[A_g]$ = global matrix for equality constraints; $\{b_g\}$ = global vector for equality constraints; $\{p^T\}$ = global vector for objective function coefficient. To avoid repetitions, the detailed formulations are not described here. For complete formulations in case of plain strain domain, one can go through Sloan (1988) and Kumar and Mohapatra (2017). A computer code is developed and implemented in MATLAB. In the present study, MOSEK toolbox is employed to solve the formulated SDP optimization problem. In past, several researchers (Krabbenhoft *et al.* 2008, Kumar and Mohapatra 2017, Ukritchon and Keawsawasvong 2019a, Ukritchon and Keawsawasvong 2019b) utilized MOSEK, which is a primal-dual interior-point solver, to perform large scale optimization with SDP.

5. Results and discussions

5.1 Comparisons

To validate the developed MATLAB code, a rigid rough strip footing having D_e/B = 0 situated on a horizontal (β = 0°) rock mass is considered under seismic loading condition. For a rock mass having GSI = 40–80, m_i = 15, $\sigma_{ci}/\gamma B$ = ∞, and D = 0, the different magnitudes of N_σ are compared with the available outcomes obtained by Saada *et al.* (2011). Saada *et al.* (2011) considered the upper bound limit analysis and utilized the following equation to determine the ultimate bearing capacity of a strip footing on a weightless rock mass

$$q_u = \frac{Q_v}{B} = \sqrt{s} N_{\sigma 0} \sigma_{ci} \tag{10}$$

where $N_{\sigma 0}$ is the bearing capacity factor that depends on the uniaxial compressive strength. In order to meet the form of Eq. (1), it can be written as $N_\sigma = \sqrt{s} N_{\sigma 0}$ for the weightless rock mass. Fig. 2(b) presents the comparison of N_σ values with different magnitudes of k_h. It can be found that the obtained N_σ values match very well with the results of Saada *et al.* (2011) for a strip footing on a horizontal rock mass subjected to seismic loading.

In the present study, for a strip footing situated on a rock slope edge having β = 30°, GSI = 50, m_i = 15, D = 0, σ_{ci} = 20 MPa, γ = 26 kN/m^3, D_e/B = 0, and B = 1 m, Table 1 demonstrates the comparison of the seismic bearing capacity (q_u) obtained from the present study with the upper bound solutions of (1) Yang (2003) based on the presumed multiwedge failure surface and the tangential Mohr-Coulomb yield criterion, (2) Saada *et al.* (2011) based on the four different types of presumed failure surfaces and the Modified Hoek-Brown yield criterion, and (3) Ausilio and Zimmaro (2015) based on the presumed log spiral failure surface and the tangential Mohr-Coulomb yield criterion (4) Maghous *et al.* (2020) based on the presumed

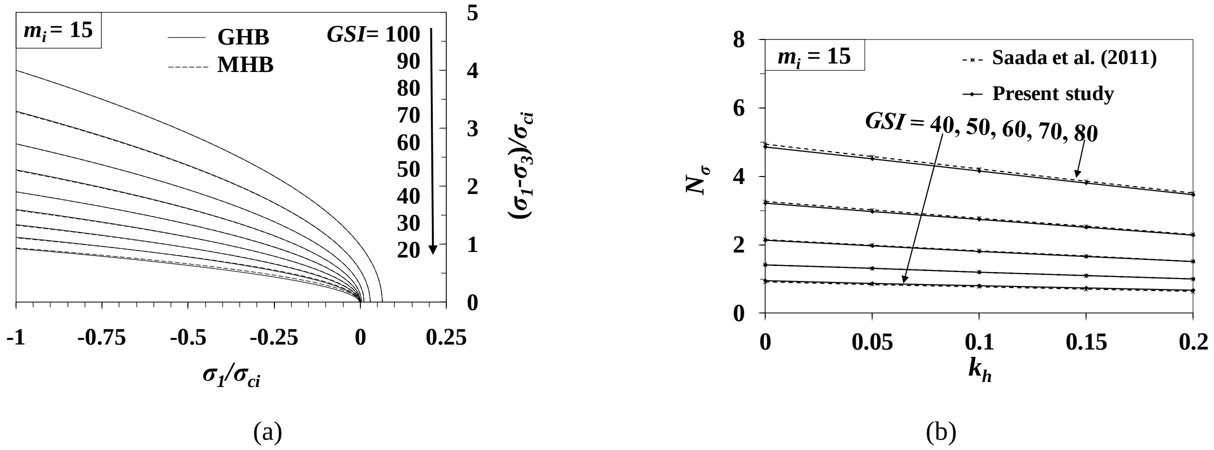

Fig. 2 (a) Comparison of strength envelopes between the MHB and the GHB yield criteria and (b) comparison of N_σ with k_h and GSI for strip footing placed on horizontal weightless rock mass having m_i = 15

Table 1 Ultimate bearing capacity (MPa) for strip footing placed at the edge (D_0 = 0) of rock slope having B = 1 m, β = 30°, D = 0, m_i =15, GSI = 50, σ_{ci} = 20 MPa, γ = 26 kN/m^3

	Present Study[a]	Yang (2009)[b]	Saada *et al*. (2011)[c]	Ausilio and Zimmaro (2015)[b]	Maghous *et al*. (2020)[c]
k_h = 0	15.27	25.456	25.430	25.960	15.572
k_h = 0.2	10.042	15.438	15.443	15.980	10.210

[a]Lower bound finite element limit analysis by following the Modified Hoek-Brown failure criterion

[b]Upper bound limit analysis by following the optimal tangential Mohr-Coulomb criterion

[c]Upper bound limit analysis by following the Modified Hoek-Brown failure criterion

multi-wedge failure surfaces and the Modified Hoek-Brown yield criterion.

It can be noted that for a strip footing placed at the edge of rock slope, the solutions of Yang (2003), Saada *et al.* (2011), and Ausilio and Zimmaro (2015) give higher values of seismic bearing capacity than the present study. This trend can be attributed due to the utilization of the upper bound limit analysis with the much simplified presumed failure surfaces in the studies mentioned above; whereas, the present study does not utilize any presumed failure surface and applies the LB-FELA with the MHB yield criterion.

In addition, it can be found that the upper bound solutions of Maghous *et al.* (2020) are very close to the solution of the present study, as Maghous *et al.* (2020) utilized the nonlinear sequential quadratic programming, presumed multi-wedge failure mechanism, and the Modified Hoek-Brown yield criterion. Thus, by comparing the results, it can be found that the present study gives the conservative q_u value for a strip footing situated horizontally on a rock slope edge.

5.2 Variation of bearing capacity factor (N_σ)

The variation in the magnitude of the bearing capacity factor (N_σ) of the strip footing situated on a rock slope edge is obtained by considering the influences of horizontal seismic acceleration coefficient (k_h), slope angle (β), Geological Strength Index (GSI), Hoek-Brown strength parameter (m_i), disturbance factor (D), normalized uniaxial compressive strength ($\sigma_{ci}/\gamma B$), and embedment depth ratio (D_e/B). Here, σ_{ci} is uniaxial compressive strength of rock mass, γ is unit weight of rock mass, and D_e is embedment depth. By varying (1) GSI values between 30 and 100, (2) m_i values between 5 and 35, (3) $\sigma_{ci}/\gamma B$ values between 125 and ∞, (4) β values between 20° and 40°, and (5) k_h values between 0.0 and 0.5, the variation in the magnitude of N_σ is obtained for three embedment depth ratios, D_e/B = 0, 1, and 2. The influences of rock strength and rock unit weight are incorporated by using $\sigma_{ci}/\gamma B$. It can be observed that an increase in unit weight causes a slight increase in the seismic bearing capacity factor, as shown in Fig. 3. As there is a little variation in the N_σ value with respect to $\sigma_{ci}/\gamma B$, Figs. 4-6 is presented to display the variation in the N_σ value with the different magnitudes of k_h for $\sigma_{ci}/\gamma B$ = 1000. In addition, by considering the effect of different D values, the variation in the magnitude of N_σ is illustrated in Fig. 7.

It is observed from Figs. 4–6 that the N_σ value decreases considerably with an increment in the value of k_h having a particular magnitude of β, GSI, m_i, D, $\sigma_{ci}/\gamma B$, and D_e/B. As expected, it is found that with the consideration of embedment depth in the strip footing, the N_σ value increases significantly.

Most importantly, it is observed that with an increase in k_h value, the reduction rate of the N_σ value decreases due to the incorporation of embedment depth. As an example, for a combination of β = 30°, GSI = 50,

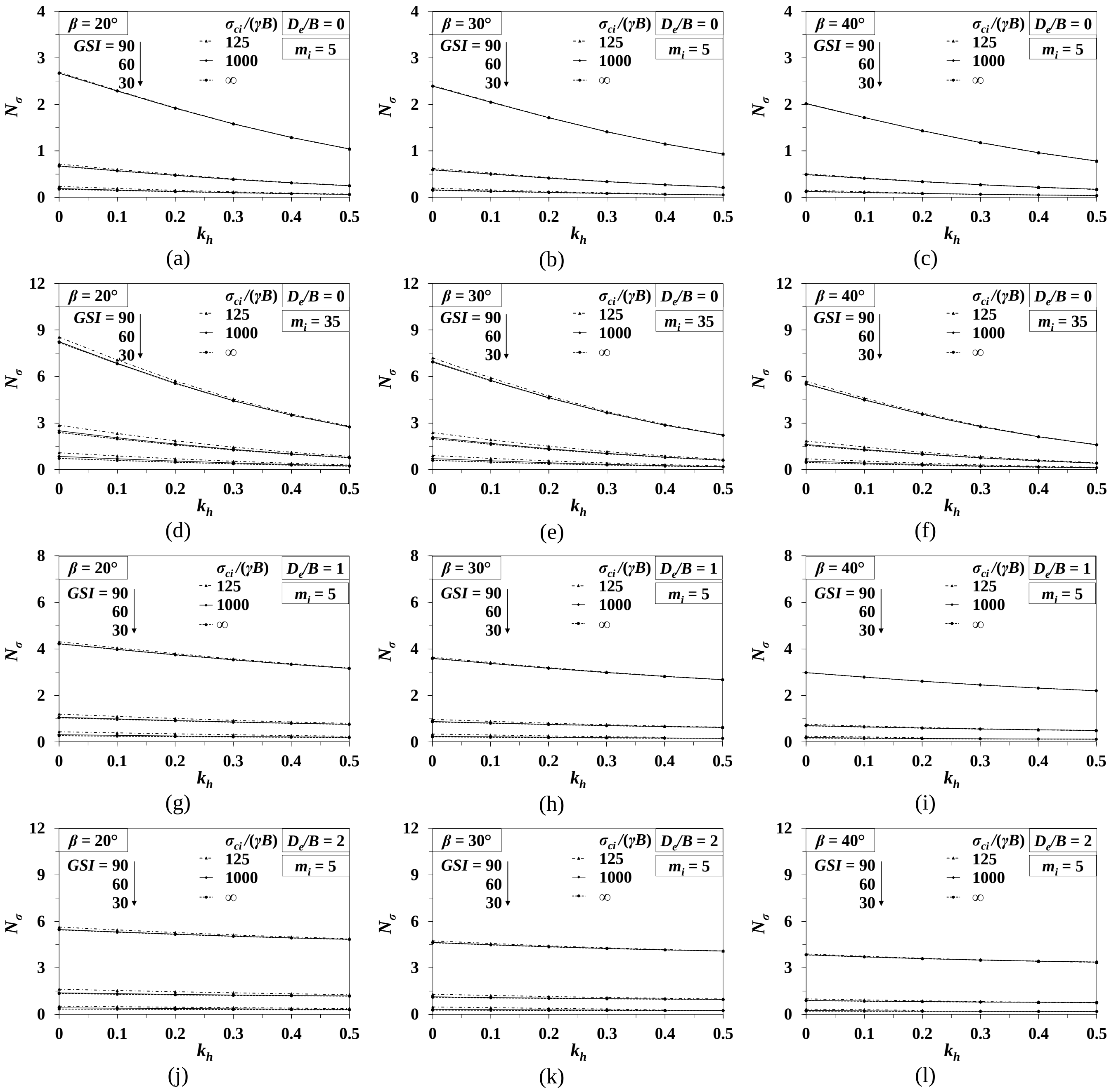

Fig. 3 For different values of GSI and $\sigma_{ci}/\gamma B$ the variation of N_σ with k_h having D = 0, (a) β = 20°, m_i = 5, D_e/B = 0, (b) β = 30°, m_i = 5, D_e/B = 0, (c) β = 40°, m_i = 5, D_e/B = 0, (d) β = 20°, m_i = 35, D_e/B = 0, (e) β = 30°, m_i = 35, D_e/B = 0, (f) β = 40°, m_i = 35, D_e/B = 0, (g) β = 20°, m_i = 5, D_e/B = 1, (h) β = 30°, m_i = 5, D_e/B = 1, (i) β = 40°, m_i = 5, D_e/B = 1, (j) β = 20°, m_i = 5, D_e/B = 2, (k) β = 30°, m_i = 5, D_e/B = 2 and (l) β = 40°, m_i = 5, D_e/B = 2

m_i = 35, $\sigma_{ci}/\gamma B$ = 1000, D = 0, D_e/B = 0, 1, and 2, the value of N_σ reduces by 71.57%, 37.68%, and 20.95%, respectively, with the change of k_h from 0 to 0.5.

It is also found that the value of N_σ decreases significantly with the increment in the magnitude of β for the predefined values of GSI, m_i, D, $\sigma_{ci}/\gamma B$, and D_e/B. In addition, an increase in the k_h value with the increment in the β value accelerates the decrement rate of N_σ value. As an example, for a combination of GSI = 90, m_i = 25, D = 0, $\sigma_{ci}/\gamma B$ = 1000, D_e/B = 1, k_h = 0, the value of N_σ decreases by 20.03% and 23.46% with the change in slope angle from 20° to 30° and 30° to 40°, respectively. In the same example, with the change in slope angle from 20° to 30° and 30° to 40° having k_h = 0.5, the value of N_σ decreases by 45.08% and 48.45%, respectively. A non-linear increment of N_σ is also observed from Figs. 4–6 with the increase in GSI value having a predefined value of β, k_h, m_i, D, $\sigma_{ci}/\gamma B$ and D_e/B. The variation in the value of N_σ is more prominent for the higher value of GSI. In contrast, the minimal variation of the N_σ is found for the lower GSI

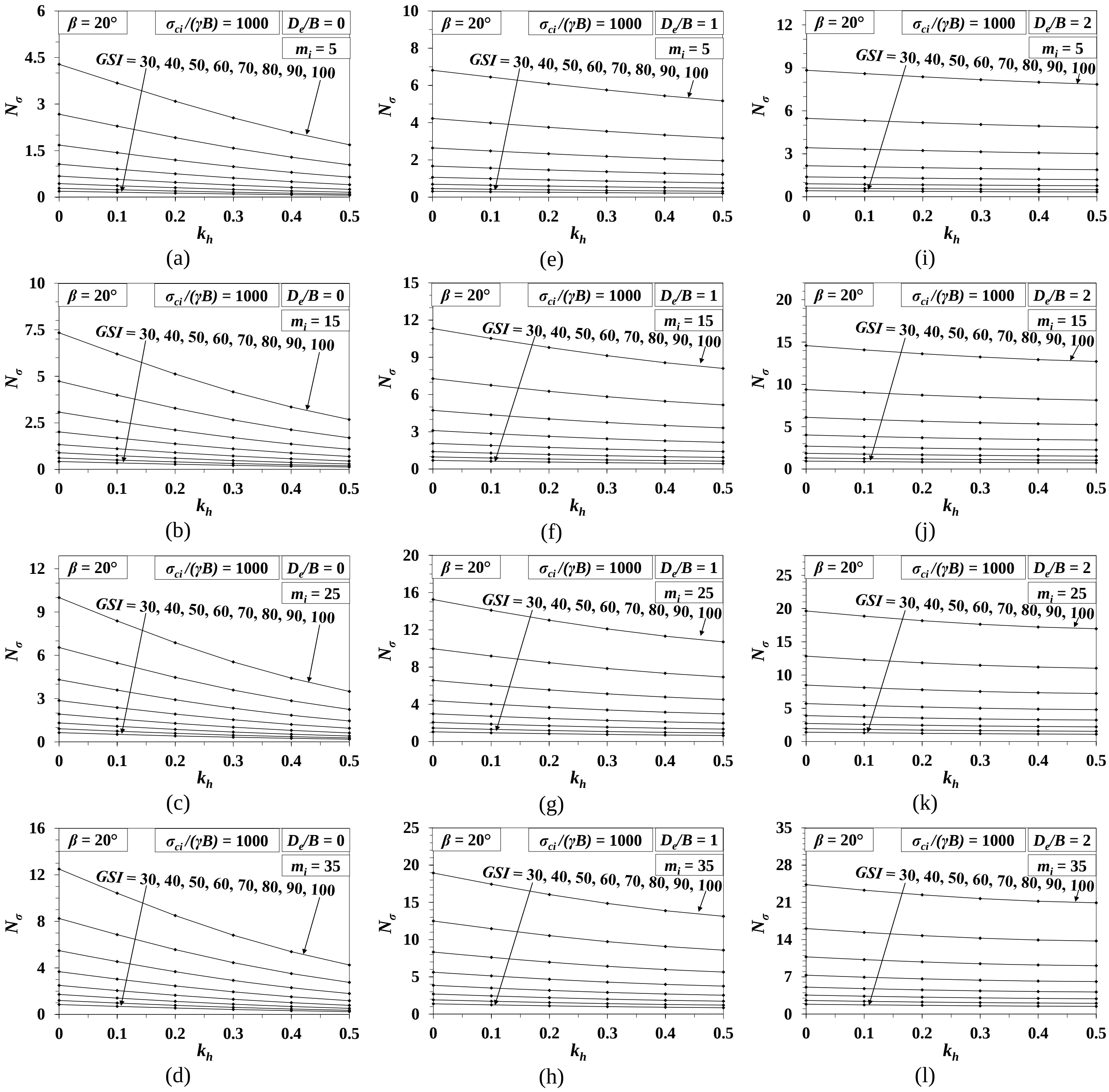

Fig. 4 For different values of GSI the variation of N_σ with k_h having $\beta = 20°$, $D = 0$, $\sigma_{ci}/\gamma B = 1000$, (a) $m_i = 5$, $D_e/B = 0$, (b) $m_i = 15$, $D_e/B = 0$, (c) $m_i = 25$, $D_e/B = 0$, (d) $m_i = 35$, $D_e/B = 0$, (e) $m_i = 5$, $D_e/B = 1$, (f) $m_i = 15$, $D_e/B = 1$, (g) $m_i = 25$, $D_e/B = 1$, (h) $m_i = 35$, $D_e/B = 1$, (i) $m_i = 5$, $D_e/B = 2$, (j) $m_i = 15$, $D_e/B = 2$, (k) $m_i = 25$, $D_e/B = 2$ and (l) $m_i = 35$, $D_e/B = 2$

value. As an example, for a strip footing having $\beta = 40°$, $k_h = 0.2$, $m_i = 15$, $D = 0$, $\sigma_{ci}/\gamma B = 1000$, $D_e/B = 1$, the value of N_σ changes from 0.303 to 6.229 with the increase in GSI value from 30 to 100. For a predefined value of β, k_h, GSI, D, $\sigma_{ci}/\gamma B$, and D_e/B, the N_σ value rises with the increment of m_i value. For instance, an embedded strip footing having $\beta = 30°$, $GSI = 70$, $D = 0$, $\sigma_{ci}/\gamma B = 1000$, $D_e/B = 1$, $k_h = 0.1$, the magnitude of N_σ changes from 1.300 to 3.954 with the variation in m_i value from 5 to 35. In the present study, it can be noticed that for an increase in the value of β, the reduction of the magnitude of N_σ can be almost overcome with the increment of D_e/B value in the presence of seismic loading. As an example, for a rock mass having $GSI = 70$, $m_i = 25$, $D = 0$, $\sigma_{ci}/\gamma B = 1000$, $D_e/B = 1$, $k_h = 0.1$, the value of N_σ decreases from 4.022 to 3.137 with the increase of β value from 20° to 30°; on the other hand, by increasing D_e/B value from 1 to 2 for $\beta = 30°$, the value of N_σ becomes 4.158. In another example, for a rock mass with $GSI = 90$, $m_i = 35$, $D = 0$, $\sigma_{ci}/\gamma B = 1000$, $k_h = 0.2$, the values of N_σ are found as 8.992 and 8.737 having the combination of $\beta = 30°$, $D_e/B = 1$, and $\beta = 40°$, $D_e/B = 2$, respectively. An increment in D_e/B value and reduction in β value show a

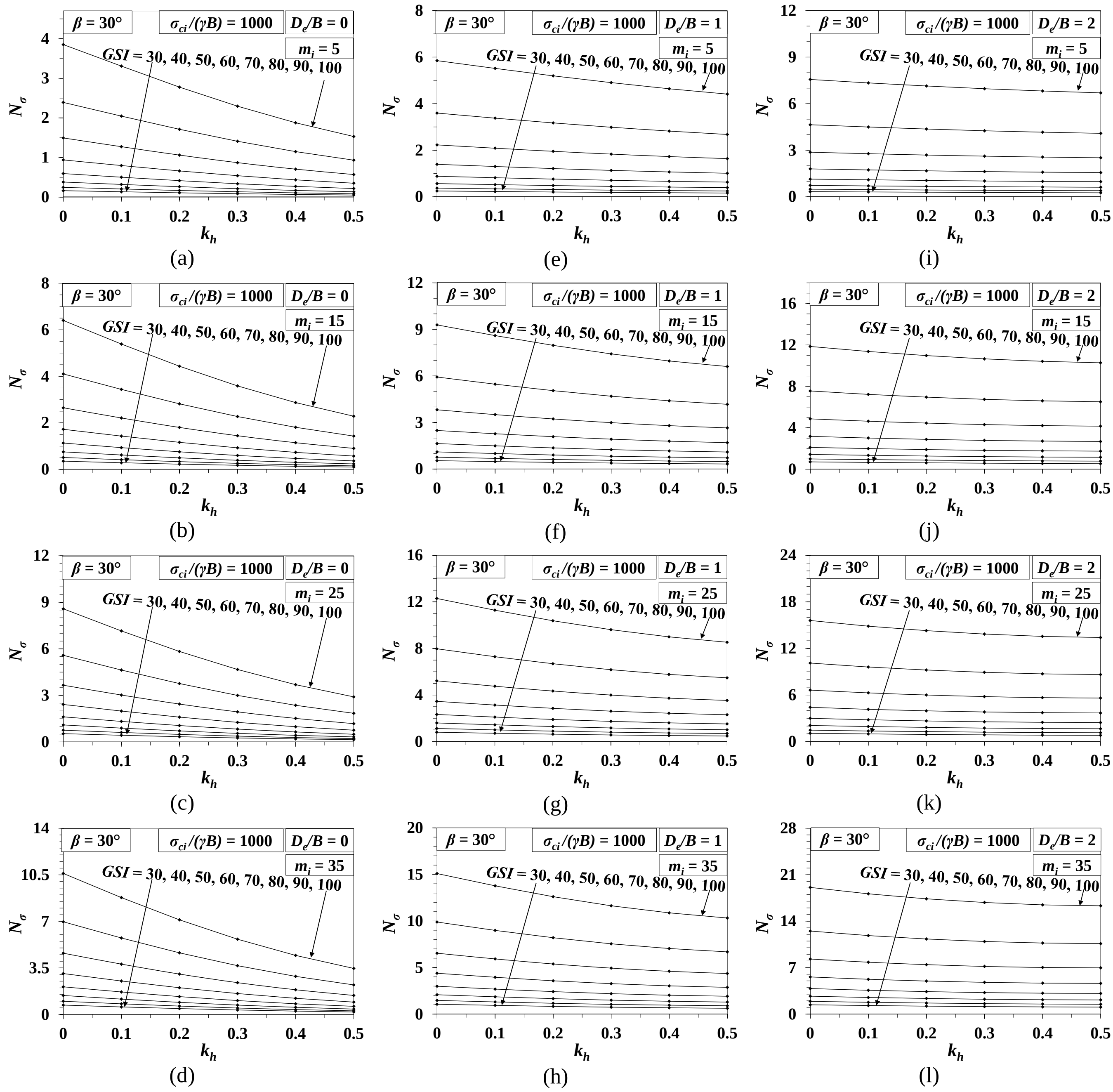

Fig. 5 For different values of *GSI* the variation of N_σ with k_h having $\beta = 30°$, $D = 0$, $\sigma_{ci}/\gamma B = 1000$, (a) $m_i = 5$, $D_e/B = 0$, (b) $m_i = 15$, $D_e/B = 0$, (c) $m_i = 25$, $D_e/B = 0$, (d) $m_i = 35$, $D_e/B = 0$, (e) $m_i = 5$, $D_e/B = 1$, (f) $m_i = 15$, $D_e/B = 1$, (g) $m_i = 25$, $D_e/B = 1$, (h) $m_i = 35$, $D_e/B = 1$, (i) $m_i = 5$, $D_e/B = 2$, (j) $m_i = 15$, $D_e/B = 2$, (k) $m_i = 25$, $D_e/B = 2$ and (l) $m_i = 35$, $D_e/B = 2$

significant increase in the N_σ value, as shown in Figs. 4–6. As the rock mass faces several disturbances throughout the construction of embedded footing, it is needed to understand the influence of disturbance factor D on the magnitude of N_σ. Therefore, for three different magnitudes of embedment depth ratio (D_e/B = 0, 1, and 2) and disturbance factor (D = 0, 0.5, and 1) of a rock mass having different *GSI* and m_i values, the changes in the magnitude of N_σ are illustrated in Fig. 7. It is found that a strip footing having predefined values of β, k_h, m_i, $\sigma_{ci}/\gamma B$, and D_e/B, the N_σ value decreases considerably for the lower values of *GSI* with the magnitude of D. In contrast, no variation in the magnitude of N_σ is found for the highest value of *GSI* (i.e., *GSI* = 100). For instance, a rock mass having $\beta = 30°$, $\sigma_{ci}/\gamma B = 1000$, $m_i = 25$, $D_e/B = 0$, $k_h = 0.2$, the magnitudes of N_σ decrease by around 88%, 84%, 80%, 72%, 62%, 48%, 27% and 0% for *GSI* = 30, 40, 50, 60, 70, 80, 90, and 100, respectively with the variation of D value from 0 to 1. The variations in the magnitude of N_σ with respect to D and k_h for rock mass having $\beta = 30°$, *GSI* = 30 and 70, m_i = 5 and 25, $\sigma_{ci}/\gamma B = 1000$, D_e/B = 0, 1 and 2 are also presented Figs. (7(g))-(7(o)).

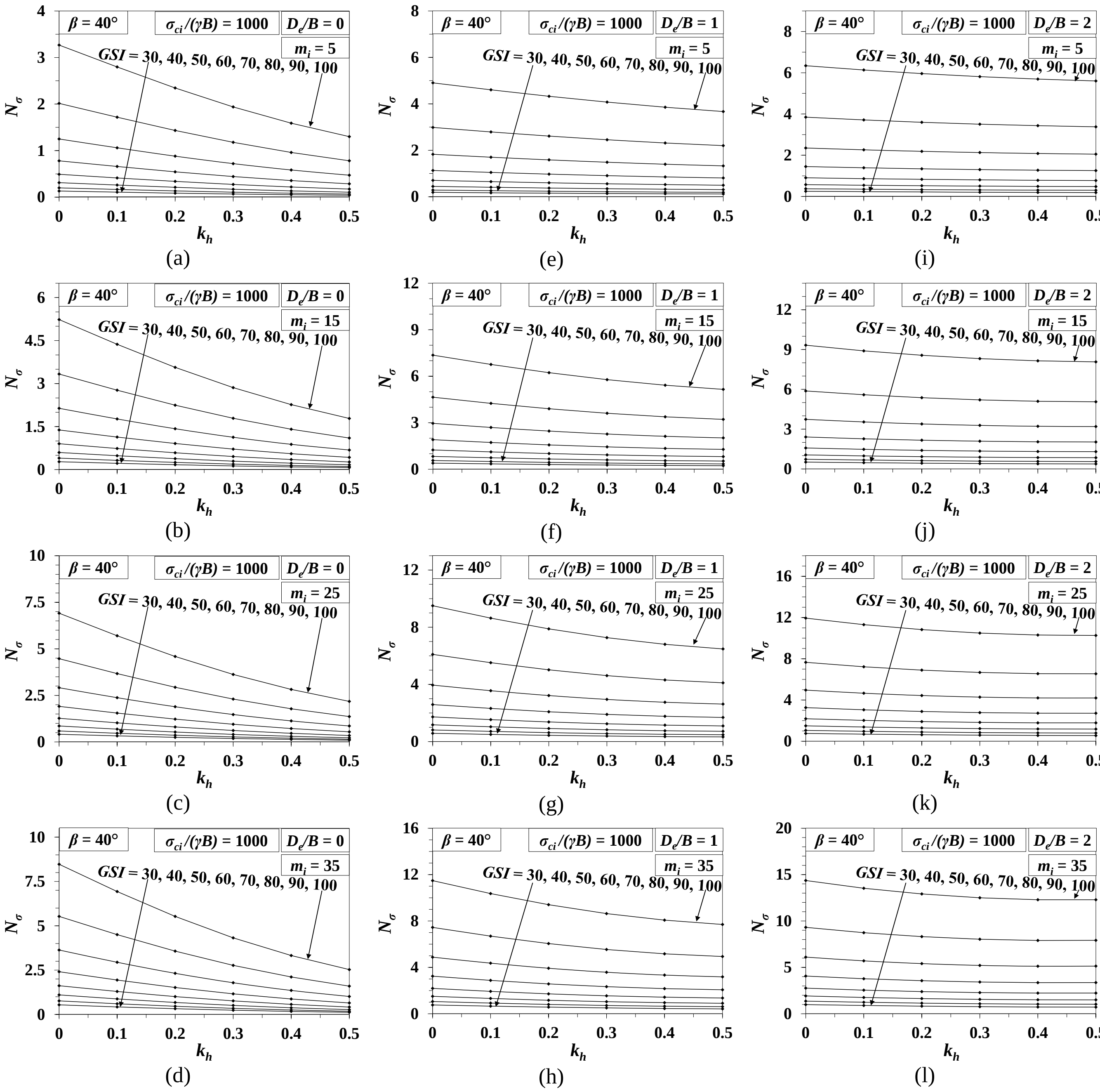

Fig. 6 For different values of *GSI* the variation of N_σ with k_h having $\beta = 40°$, D = 0, $\sigma_{ci}/\gamma B$ = 1000, (a) m_i = 5, D_e/B = 0, (b) m_i = 15, D_e/B = 0, (c) m_i = 25, D_e/B = 0, (d) m_i = 35, D_e/B = 0, (e) m_i = 5, D_e/B = 1, (f) m_i = 15, D_e/B = 1, (g) m_i = 25, D_e/B = 1, (h) m_i = 35, D_e/B = 1, (i) m_i = 5, D_e/B = 2, (j) m_i = 15, D_e/B = 2, (k) m_i = 25, D_e/B = 2 and (l) m_i = 35, D_e/B = 2

5.3 Failure patterns

With respect to shear failure, the stress state at each node of the triangular element is calculated by using a/d ratio; here, $a = (\sigma_1 - \sigma_3)$ and $d = (-\sigma_{ci} m_b \sigma_1 + s)^{0.5}$. For a point at plastic-state, the magnitude of a/d becomes to 1; whereas, for a point at non-plastic state, the magnitude of a/d becomes less than 1. For an embedded strip footing, the stress state are illustrated in Figs. 8 and 9 for two different slope angles, namely, β = 30°, and 40°, having k_h = 0, 0.1 and 0.2, *GSI* = 30, m_i = 5, $\sigma_{ci}/\gamma B$ = 1000, D = 0, and D_e/B = 0, 1, and 2. For all failure patterns, it is found that a non-yielding wedge exists just below the footing. It is also found that the area of plastic zone, below and around the footing, reduces with the increase in the slope angle. On the other hand, the spreading of plastic zone escalates along the slope face with the increment in the embedment depth, as shown in Figs. 8 and 9.

In addition, it is found that for a rock slope having $\beta \geq 30°$ and poor strength (lesser *GSI* and m_i), a stressed zone starts to develop near the toe with the existence of seismic loading. It indicates that with the increase in the slope angle and seismic loading, slope started to become unstable.

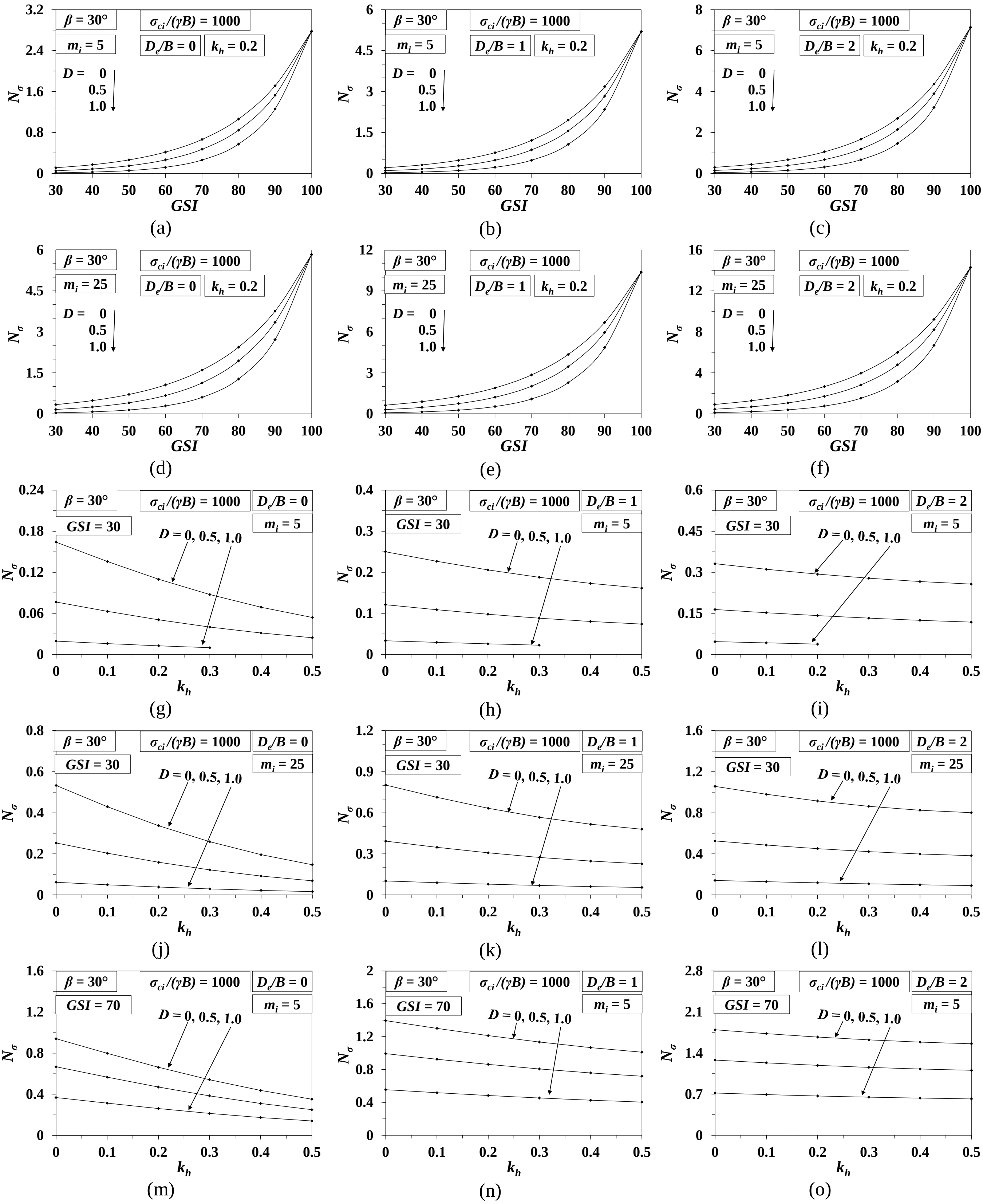

Fig. 7 Effect of disturbance factor on N_σ having different values of *GSI* for $\beta = 30°$, $k_h = 0.2$, $\sigma_{ci}/\gamma B = 1000$, (a) $m_i = 5$, $D_e/B = 0$, (b) $m_i = 5$, $D_e/B = 1$, (c) $m_i = 5$, $D_e/B = 2$, (d) $m_i = 25$, $D_e/B = 0$, (e) $m_i = 25$, $D_e/B = 1$, (f) $m_i = 25$, $D_e/B = 2$; effect of disturbance factor on N_σ having different values of k_h for $\beta = 30°$, $\sigma_{ci}/\gamma B = 1000$, (g) $GSI = 30$, $m_i = 5$, $D_e/B = 0$, (h) $GSI = 30$, $m_i = 5$, $D_e/B = 1$, (i) $GSI = 30$, $m_i = 5$, $D_e/B = 2$, (j) $GSI = 30$, $m_i = 25$, $D_e/B = 0$, (k) $GSI = 30$, $m_i = 25$, $D_e/B = 1$, (l) $GSI = 30$, $m_i = 25$, $D_e/B = 2$, (m) $GSI = 70$, $m_i = 5$, $D_e/B = 0$, (n) $GSI = 70$, $m_i = 5$, $D_e/B = 1$ and (o) $GSI = 70$, $m_i = 5$, $D_e/B = 2$

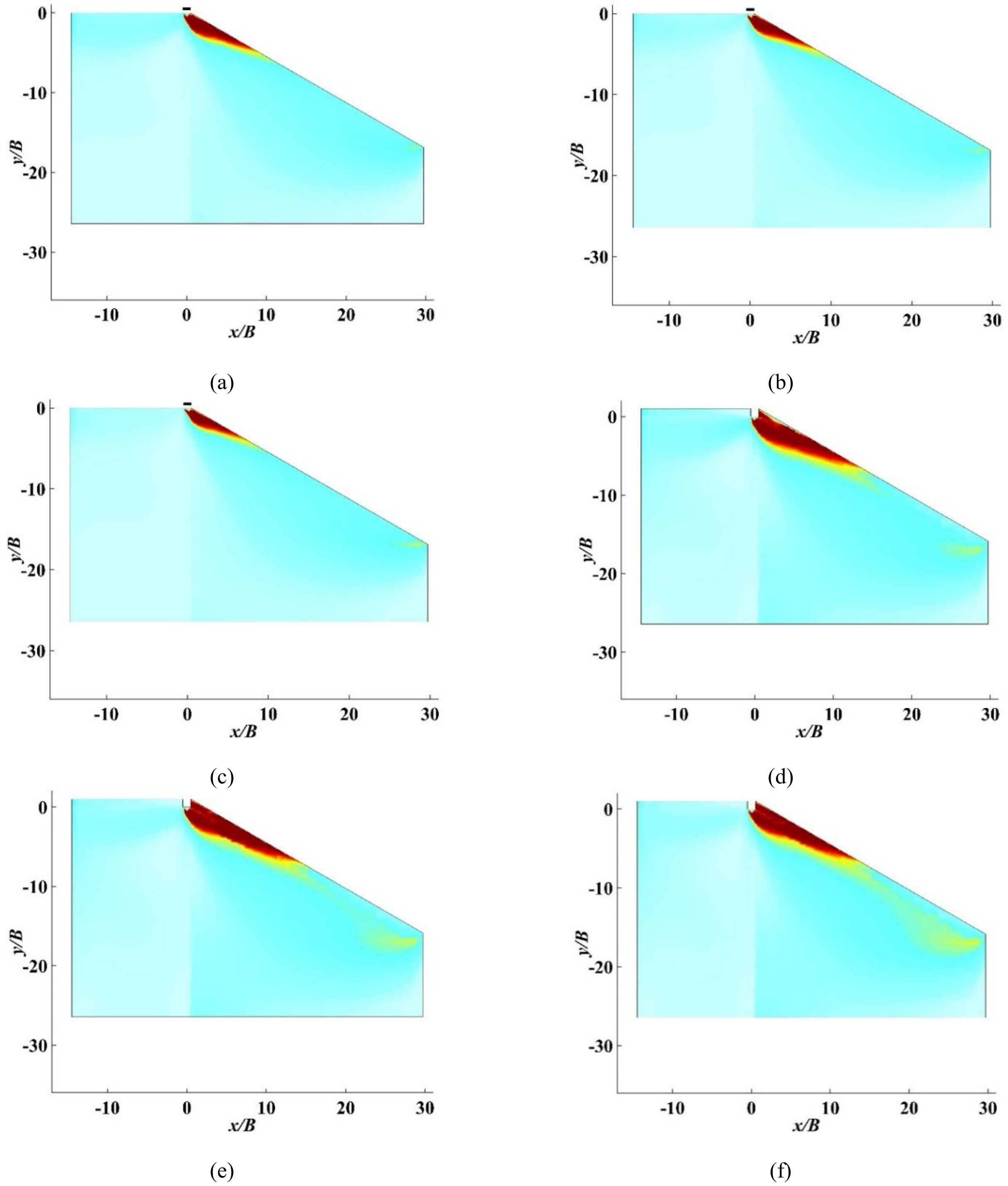

Fig. 8 Failure patterns for GSI = 30, m_i = 5, D = 0, $\sigma_{ci}/\gamma B$ = 1000, β = 30°, (a) k_h = 0.0, D_e/B = 0, (b) k_h = 0.1, D_e/B = 0, (c) k_h = 0.2, D_e/B = 0, (d) k_h = 0.0, D_e/B = 1, (e) k_h = 0.1, D_e/B = 1 and (f) k_h = 0.2, D_e/B = 1

6. Remarks

In the present study, the seismic bearing capacity of an embedded strip footing situated on the rock slope is determined by using the LB-FELA in conjunction with the SDP. Here, the failure of rock mass is modelled as the MHB yield criterion by setting the value of α as 0.5 (Kumar and Mohapatra 2017). As mentioned previously, the adopted approximation gives a consistent result for the GSI values between 30 and 100. Recently, a new methodology has been presented by Kumar and Rahaman (2020) to overcome the optimization shortcoming for lower GSI values. In that study, the failure of the rock mass was modelled by following the GHB yield criterion with the implementation of the power cone programming (PCP) in the LB-FELA framework. However, the present study does not deal with the PCP in the LB-FELA framework.

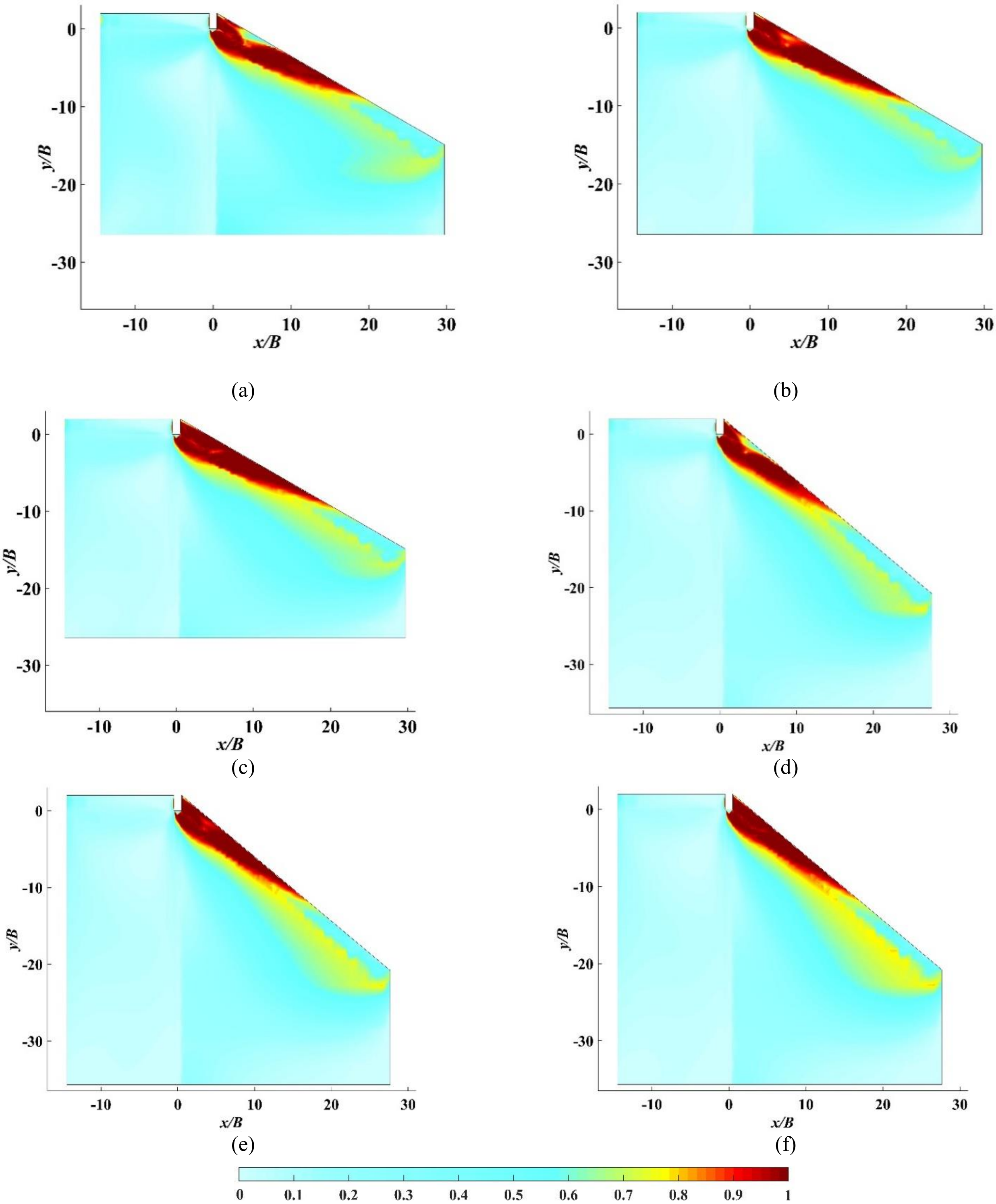

Fig. 9 Failure patterns for GSI = 30, m_i = 5, D = 0, $\sigma_{ci}/\gamma B$ = 1000, D_e/B = 2, (a) k_h = 0.0, β = 30°, (b) k_h = 0.1, β = 30°, (c) k_h = 0.2, β = 30°, (d) k_h = 0.0, β = 40°, (e) k_h = 0.1, β = 40° end (f) k_h = 0.2, β = 40°

Therefore, it can be considered as a limitation of the present study.

7. Conclusions

To obtain the bearing capacity of an embedded strip footing situated on rock slope edge under seismic loading, an extensive numerical investigation is carried out in the present study. The bearing capacity factor (N_σ) for the variation of horizontal seismic acceleration coefficient (k_h), slope angle (β), Geological Strength Index (GSI), Hoek-Brown material constant (m_i), disturbance factor (D), depth of the embedment (D_e), and normalized uniaxial compressive strength ($\sigma_{ci}/\gamma B$) is computed by employing MHB yield criterion. The LB-FELA in combination with the semidefinite programming is used to perform the analysis. The maximum value of N_σ for a strip footing can be achieved with higher values of *GSI* and m_i having a less steep slope under static loading condition. An increment in the magnitude of k_h shows a considerable reduction in the value of N_σ. Further reduction in the magnitude of N_σ is found with the increase in β value. The magnitude of N_σ increases with the increase in the embedment depth of the strip footing. On the other hand, an increment in the value of disturbance factor shows a significant reduction in the value of N_σ. Further, the stress contour plots are also presented to examine the combined failure mechanism of the footing–rock slope system under static as well as seismic loading conditions. The generated design charts are likely to be beneficial to carry out the bearing capacity of the embedded footing placed on a rock slope in the presence of seismic loading.

References

Alencar, A.S., Galindo, R.A. and Melentijevic, S. (2019), "Bearing capacity of foundation on rock mass depending on footing shape and interface roughness", *Geomech. Eng.*, **18**(4), 391-406. https://doi.org/10.12989/gae.2019.18.4.391.

Alencar, A.S., Galindo, R.A. and Melentijevic, S. (2020), "Bearing capacity of shallow foundations on the bilayer rock", *Geomech. Eng.*, **21**(1), 11-21. https://doi.org/10.12989/gae.2020.21.1.011.

Ausilio, E. and Zimmaro, P. (2015), "Displacement-based seismic design of a shallow strip footing positioned near the edge of a rock slope", *Int. J. Rock Mech. Min. Sci*., **76**, 68-77. https://doi.org/10.1016/j.ijrmms.2015.02.010.

Azzouz, A.S. and Baligh, M.M. (1983), "Loaded areas on cohesive slopes", *J. Geotech. Eng*., **109**(5), 724-729. https://doi.org/10.1061/(ASCE)0733-9410(1983)109:5(724).

Baker, R., Shukha, R., Operstein, V. and Frydman, S. (2006), "Stability charts for pseudo-static slope stability analysis", *Soil Dyn. Earthq. Eng.*, **26**(9), 813-823. https://doi.org/10.1016/j.soildyn.2006.01.023.

Budhu, M. and Al-Karni, A. (1993), "Seismic bearing capacity of soils", *Geotechnique*, **43**(1), 181-187. https://doi.org/10.1680/geot.1993.43.1.181.

Casablanca, O., Biondi, G., Cascone, E. and Filippo, G.D. (2021), "Static and seismic bearing capacity of shallow strip foundations on slopes", *Geotechnique*, 1-15. https://doi.org/10.1680/jgeot.20.P.044.

Castelli, F. and Lentini, V. (2012), "Evaluation of the bearing capacity of footings on slopes", *Int. J. Phy. Model. Geotech.*, **12**(3), 112-118. https://doi.org/10.1680/ijpmg.11.00015.

Chakraborty, D. and Kumar, J. (2015), "Seismic bearing capacity of shallow embedded foundations on a sloping ground surface", *Int. J. Geomech.*, **15**(1), 04014035. https://doi.org/10.1061/(ASCE)GM.1943-5622.0000403.

Georgiadis, K. (2010), "Undrained bearing capacity of strip footings on slopes", *J. Geotech. Geoenviron Eng*., **136**(5), 677-685. https://doi.org/10.1061/(ASCE)GT.1943-5606.0000269.

Halder, K. and Chakraborty, D. (2020), "Probabilistic bearing capacity of strip footing on reinforced anisotropic soil slope", *Geomech. Eng*., **23**(1), 15-30. https://doi.org/10.12989/gae.2020.23.1.015.

Hoek, E., Carranza–Torres, C. and Corkum, B. (2002), "Hoek–Brown failure criterion–2002", *Proceedings of NARMS-Tac*., **1**(1), 267-273.

Hynes-Griffin, M.E. and Franklin, A.G. (1984), "Rationalizing the seismic coefficient method", *Miscellaneous Paper GL-84-13*, U.S. Army Corps. Eng. Vicksburg Miss.

Karray, M., Hussien, M.N., Delisle, M.C. and Ledoux, C. (2018), "Framework to assess pseudo-static approach for seismic stability of clayey slopes", *Can. Geotech. J.*, **55**(12), 1860-1876. https://doi.org/10.1139/cgj-2017-0383.

Keshavarz, A., Fazeli, A. and Sadeghi, S. (2016), "Seismic bearing capacity of strip footings on rock masses using the Hoek–Brown failure criterion", *J. Rock Mech. Geotech. Eng*., **8**(2), 170-177. https://doi.org/10.1016/j.jrmge.2015.10.003.

Keskin, M.S. and Laman, M. (2014), "Experimental study of bearing capacity of strip footing on sand slope reinforced with tire chips", *Geomech. Eng*., **6**(3), 249-262. https://doi.org/10.12989/gae.2014.6.3.249.

Krabbenhoft, K., Lyamin, A.V. and Sloan, S.W. (2008), "Three-dimensional Mohr–Coulomb limit analysis using semidefinite programming", *Commun. Num. Meth. Eng.*, **24**(11), 1107-1119. https://doi.org/10.1002/cnm.1018.

Kramer, S.L. (1996), *Geotechnical earthquake engineering*, Prentice Hall, New Jersey

Kumar, J. and Ghosh, P. (2006), "Seismic bearing capacity for embedded footings on sloping ground", *Geotechnique*, **56**(2), 133-140. https://doi.org/10.1680/geot.2006.56.2.133.

Kumar, J. and Mohan Rao, V.B.K. (2003), "Discussion-Seismic bearing capacity factors for spread foundation", *Geotechnique*, **53**(4), 445-446. https://doi.org/10.1680/geot.2003.53.4.445.

Kumar, J. and Mohapatra, D. (2017), "Lower-bound finite elements limit analysis for Hoek-Brown materials using semidefinite programming", *J. Eng. Mech.*, **143**(9), 04017077. https://doi.org/10.1061/(ASCE)EM.1943-7889.0001296.

Kumar, J. and Rahaman, O. (2020), "Lower bound limit analysis using power cone programming for solving stability problems in rock mechanics for generalized Hoek–Brown criterion", *Rock Mech. Rock Eng*., **53**(7), 3237-3252. https://doi.org/10.1007/s00603-020-02099-y.

Lyamin, A.V., Yu, H.S., Sloan, S.W. and Hossain, M.Z. (1998), "Lower bound limit analysis for jointed rocks using the Hoek-Brown yield criterion", *Aus. Geomech. J.*, **33**(1), 46-62.

Lysmer, J. (1970), "Limit analysis of plane problems in soil mechanics", *J. Soil Mech. Found. Div.*, **96**(4), 1311-1334.

Maghous, S., Saada, Z., Garnier, D. and Dutra, V.F.P. (2020), "Upper bound kinematic approach to seismic bearing capacity of strip foundations resting near rock slopes", *Eur. J. Environ. Civ. Eng.*, 1-24. https://doi.org/10.1080/19648189.2020.1830179.

Marcuson, W.F. (1981), "Moderator's report for session on Earth Dams and Stability of Slopes under Dynamic Loads", *Proceedings of the Int. Conf. Recent Adv. Geotech. Earthq. Eng. Soil Dyn.*, **3**, 1175.

MATLAB R2015a (2015), [Computer software]. Natick, MA, MathWorks.

Merifield, R.S., Lyamin, A.V. and Sloan, S.W. (2006), "Limit analysis solutions for the bearing capacity of rock masses using the generalized Hoek–Brown criterion", *Int. J. Rock Mech. Min. Sci.*, **43**(6), 920-937. https://doi.org/10.1016/j.ijrmms.2006.02.001.

Meyerhof, G.G. (1963), "Some recent research on the bearing capacity of foundations", *Can. Geotech. J.*, **1**(1), 16-26. https://doi.org/10.1139/t63-003.

MOSEK ApS, version 9.0 [Computer software]. MOSEK, Copenhagen, Denmark.

Rahaman, O. and Kumar, J. (2020), "Stability analysis of twin horse-shoe shaped tunnels in rock mass", *Tunn. Undergr. Sp.*

Tech., **98**, 103354. https://doi.org/10.1016/j.tust.2020.103354.
Saada, Z., Maghous, S. and Garnier, D. (2011), "Seismic bearing capacity of shallow foundations near rock slopes using the generalized Hoek–Brown criterion", *Int. J. Numer. Anal. Meth. Geomech.*, **35**(6), 724-748. https://doi.org/10.1002/nag.929.
Sarma, S.K. and Iossifelis, I.S. (1990), "Seismic bearing capacity factors of shallow strip footings", *Geotechnique*, **40**(2), 265-273. https://doi.org/10.1680/geot.1990.40.2.265.
Seed, H.B. (1979), "Considerations in the earthquake-resistant design of earth and rockfill dams", *Geotechnique*, **29**(3), 215-263. https://doi.org/10.1680/geot.1979.29.3.215.
Shields, D., Chandler, N. and Garnier, J. (1990), "Bearing capacity of foundations in slopes." *J. Geotech. Eng.*, **116**(3), 528-537. https://doi.org/10.1061/(ASCE)0733-9410(1990)116:3(528).
Shukla, R.P. and Jakka, R.S. (2018), "Critical setback distance for a footing resting on slopes under seismic loading", *Geomech. Eng.*, **15**(6), 1193-1205. https://doi.org/10.12989/gae.2018.15.6.1193.
Sloan, S.W. (1988), "Lower bound limit analysis using finite elements and linear programming", *Int. J. Num. Anal. Meth. Geomech.*, **12**(1), 61-67. https://doi.org/10.1002/nag.1610120105.
Terzaghi, K. (1950), *Mechanisms of landslides*, Engineering Geology (Berkey) Volume, Geol. Soc. Am.
Ukritchon, B. and Keawsawasvong, S. (2019a), "Lower bound stability analysis of plane strain headings in Hoek-Brown rock masses", *Tunn. Undergr. Sp. Tech.*, **84**, 99-112. https://doi.org/10.1016/j.tust.2018.11.002.
Ukritchon, B. and Keawsawasvong, S., (2019b), "Stability of unlined square tunnels in Hoek-Brown rock masses based on lower bound analysis", *Comput. Geotech.*, **105**, 249-264. https://doi.org/10.1016/j.compgeo.2018.10.006.
Wu, G., Zhao, M. and Zhao, H. (2021), "Undrained seismic bearing capacity of strip footings horizontally embedded in two-layered slopes", *Earthq. Spectra*., **37**(2), 637-651. https://doi.org/10.1177/8755293020957332.
Xiao, Y., Zhao, M., Zhang, R., Zhao, H. and Wu, G. (2019), "Stability of dual square tunnels in rock masses subjected to surcharge loading", *Tunn. Undergr. Sp. Tech.*, **92**, 103037. https://doi.org/10.1016/j.tust.2019.103037.
Yang, S., Leshchinsky, B., Cui, K., Zhang, F. and Gao, Y. (2021), "Influence of failure mechanism on seismic bearing capacity factors for shallow foundations near slopes." *Geotechnique*, 1-14. https://doi.org/10.1680/jgeot.19.P.329.
Yang, X., Yin, J.H. and Li, L. (2003), "Influence of a non-linear failure criterion on the bearing capacity of a strip footing resting on rock mass using a lower bound approach", *Can. Geotech. J.*, **40**(3), 702-707. https://doi.org/10.1139/t03-010.
Yang, X.L. (2009), "Seismic bearing capacity of a strip footing on rock slopes", *Can. Geotech. J.*, **46**(8), 943-954. https://doi.org/10.1139/T09-038.
Zhang, R., Xiao, Y., Zhao, M. and Zhao, H. (2019), "Stability of dual circular tunnels in a rock mass subjected to surcharge loading", *Comput. Geotech.*, **108**, 257-268. https://doi.org/10.1016/j.compgeo.2019.01.004

CC

Table A1 Recommended magnitude of the horizontal seismic acceleration coefficient k_h (Kramer 1996)

Recommended by	Description	Recommended magnitude of k_h	Factor of Safety
Terzaghi (1950)	Severe Earthquake	0.1	-
	Violent and destructive Earthquake	0.2	
	Catastrophic	0.5	
Seed (1979)	Richter's magnitude 6.5	0.1	$\geq$ 1.15
	Richter's magnitude 8.5	0.15	
Marcuson (1981)	For earth dam	1/3 to 1/2 of a_{max}/g	> 1.0
Hynes-Griffin and Franklin (1984)	Conclusion drawn based on 350 accelerograms data	$0.5a_{max}/g$	> 1.0

Here, a_{max}/g = Peak Horizontal Acceleration

Appendix A

A.1 Remarks regarding the presence of k_v

From the superstructure, a vertical downward static load $V = mg$ acts at the footing base. In the existence of both vertical and horizontal seismic accelerations, an additional vertical structural load of magnitude $k_v mg$ needs to be considered into the calculation. Thus, the total vertical downward structural load becomes $(1 + k_v)mg$ with the existence of downward seismic acceleration $(+ k_v g)$. In contrast, with the presence of seismic upward acceleration $(- k_v g)$, the total vertical structural load becomes $(1 - k_v)mg$ in the downward direction. In addition, due to the presence of horizontal seismic acceleration, a total horizontal load of magnitude $k_h mg$ also needs to be considered at the footing base.

Similarly, the horizontal body force and vertical downward force per unit volume also present throughout the domain. The magnitudes of the two forces can be expressed as $k_h\gamma$ and $(1 \pm k_v)\gamma$, respectively.

As described earlier, the total vertical downward force at the base of the footing can be written as

$$Q_v = (1 \pm k_v)mg \tag{A.1}$$

At the footing base, the horizontal force can be considered as

$$k_h^* Q_v = k_h mg \tag{A.2}$$

where, k_h^* is the modified value of k_h

Thus, from Equations (A.1) and (A.2), k_h^* can be written as

$$k_h^* = \frac{k_h}{(1 \pm k_v)} \tag{A.3}$$

By following the same principle for the body forces per unit volume, which is acting along the horizontal and vertical downward directions, the revised magnitude of unit weight can be written as

$$\gamma^* = (1 \pm k_v)\gamma \tag{A.4}$$

$$k_h^* \gamma^* = k_h \gamma \tag{A.5}$$

Therefore, separate analysis is not needed in the presence of both k_h and k_v; only the consideration of k_h can serve the purpose. The ultimate bearing capacity can be determined by following the modification in the magnitudes of the unit weight (γ to γ^*) and horizontal seismic acceleration (k_h to k_h^*). From the design chart, one can easily find out the magnitude of the N_σ corresponding to the magnitude of k_h^*. As the present study determines the ultimate bearing capacity of the strip footing ($q_u = N_\sigma \sigma_{ci}$) by using the non-dimensional parameter $\sigma_{ci}/\gamma B$, the magnitude of σ_{ci} needs to be modified corresponding to the revised magnitude of unit weight. As an example, for k_h = 0.25 and $k_v = -0.5k_h$, the magnitude of k_h^* becomes 0.29 by following Equation (A.3). Similarly, for k_h = 0.25 and $k_v = +0.5k_h$, the value of k_h^* becomes 0.22. For a strip footing having $\beta = 20°$, $D_e/B = 0$, $GSI = 90$, $m_i = 25$, $D = 0$, $\sigma_{ci}/\gamma B = 1000$, the non-dimensional bearing capacity factor, N_σ can be calculated as 3.678 and 4.274 from Fig. 4(c) corresponding to the revised k_h (i.e., k_h^*) magnitudes of 0.29 and 0.22, respectively. The magnitude of N_σ is 4.039 with k_h = 0.25, for k_v = 0.0. Additionally, for a rock mass having γ = 26 kN/m^3 and σ_{ci} = 26 MPa in the presence of k_v = – 0.125 and k_v = + 0.125, the corresponding magnitudes of γ^* become 22.75 kN/m^3 and 29.25 kN/m^3, respectively. Now, in the present study, for the strip footing having B = 1 m, the revised $\sigma_{ci} = 1000\gamma^* B$ values are 22.75 MPa and 29.25 MPa, respectively. Therefore, with k_h = 0.25 for k_v = – 0.125, 0.0, + 0.125, the magnitudes of $q_u = N_\sigma \sigma_{ci}$ are 83.67 MPa, 105.01 MPa and 125.02 MPa, respectively. It needs to be mentioned here that similar type of formulation was previously utilized by Kumar and Rao (2003) to incorporate the effect of pseudo static vertical seismic accelerations for strip footing on a soil slope.

A.2 Selection of k_h for design

As per Kramer (1996), there is no fixed rule to select the appropriate horizontal seismic acceleration coefficient k_h for design. The seismic acceleration coefficients are generally calculated from experience as recommended by several researchers (Terzaghi 1950, Seed 1979, Marcuson 1981, Hynes-Griffin and Franklin 1984) either with the help of the peak ground acceleration or the maximum horizontal acceleration of an earthquake (refer to Table A1). In addition, the present study allows to consider the effects of the both vertical and horizontal seismic acceleration coefficients (k_v and k_h) by using the modified horizontal seismic acceleration coefficient (k_h^*). As shown in the previous section, the magnitude of k_h^* becomes higher value than the magnitude of k_h with the presence of seismic upward acceleration ($-k_v g$). Therefore, in the present study, the range of horizontal seismic acceleration coefficient k_h is considered between 0 and 0.5.